applied sciences

MDPI

Article

Experimental and Numerical Investigation of a Method for Strengthening Cold-Formed Steel Profiles in Bending

Ehsan Taheri [1,*], Ahmad Firouzianhaji [1], Peyman Mehrabi [2], Bahador Vosough Hosseini [3] and Bijan Samali [1]

[1] Centre for Infrastructure Engineering, Western Sydney University, Sydney, Kingswood, NSW 2747 Australia; a.firouzianhaji@westernsydney.edu.au (A.F.); b.samali@westernsydney.edu.au (B.S.)
[2] Department of Civil Engineering, K.N. Toosi University of Technology, Tehran, Mirdamad 15875-4416, Iran; peyman804m@gmail.com
[3] School of Civil, Mining and Environmental Engineering, University of Wollongong, NSW 2500, Australia; ben.vosough@yahoo.com
* Correspondence: e.taheri@westernsydney.edu.au

Received: 28 April 2020; Accepted: 25 May 2020; Published: 1 June 2020

Abstract: Perforated cold-formed steel (CFS) beams subjected to different bending scenarios should be able to deal with different buckling modes. There is almost no simple way to address this significant concern. This paper investigates the bending capacity and flexural behavior of a novel-designed system using bolt and nut reinforcing system through both experimental and numerical approaches. For the experiential program, a total of eighteen specimens of three types were manufactured: a non-reinforced section, and two sections reinforced along the upright length at 200 mm and 300 mm pitches. Then, monotonic loading was applied to both the minor and major axes of the specimens. The finite element models were also generated and proved the accuracy of the test results. Using the proposed reinforcing system the flexural capacity of the upright sections was improved around either the major axis or minor axis. The 200 mm reinforcement type provided the best performance of the three types. The proposed reinforcing pattern enhanced flexural behavior and constrained irregular buckling and deformation. Thus, the proposed reinforcements can be a very useful and cost-effective method for strengthening all open CFS sections under flexural loading, considering the trade-off between flexural performance and the cost of using the method.

Keywords: cold-formed steel; upright; monotonic loading

1. Introduction

Steel pallet racking systems have been widely used around the world since the industrial revolution. Over the years, steel pallet racking has evolved from hot-rolled profiles to cold-formed steel (CFS) profiles in order to increase the structural performance in terms of engineering optimization. The benefit of steel pallet racking is its flexibility in using limited space in warehouses. The increase in popularity of steel storage racking means more types of applications are now required to meet the demands of customers [1]. However, the performance of the proposed sections needs to be well understood by full-scale testing. Generally, perforated CFS components are susceptible to bending forces. Following the previous study on the flexural behavior of the perforated CFS profiles, these sections have been subjected to cyclic and monotonic forces where they have experienced different kinds of deformations, notably different types of buckling [2]. There are three primary types of buckling modes for CFS sections including local, distortional and global. Therefore, it is vital to find suitable ways to speed up constraining the buckling process.

Yu and Schafer [3] and Calderoni et al. [4] performed a series of four-point bending tests to investigate the distortional and flexural performance of C and Z-shaped section built-up cold-formed steels. Rogers et al. [5] evaluated the bending moment of existing authentic experimental results with different code provisions. Hancock et al. [6] proposed a new design approach of distortional buckling strength for C and Z-shaped cold-formed steel sections. Wang et al. [7] experimentally and analytically investigated C-shaped cold-formed steel beams with or without edge stiffeners. Using the stiffeners significantly enhanced the flexural stiffness and buckling resistivity of the beam under pure and non-pure bending tests. Wang et al. [8] performed a four-point bending test program on cold-formed steel built-up section beams with web perforations. Local geometric imperfections were also measured. When the hole diameter to web depth ratio (d_h/d_w) increased from 0.25 to 0.5, the moment rotation capacity reduced slightly by 6%. However, increasing the ratio up to 0.7 reduced the capacity by 16%. The effects of the web–hole ratio on the performance of the perforated cold-formed steel channel section beams were experimentally and analytically investigated. The greater the increase in the hole area, the more reduction in the ultimate distortional buckling moment [9–14]. The reported results also illustrated that the size of the web holes directly affected the distortional buckling moment, with the bigger the hole, the lower the buckling moment. Zhou et al. [15] examined the authenticity of the Australia/New Zealand Standard (AS 1391) on the flexural strength design of rectangular tubes manufactured with cold-rolling steel, where the Australian standard has shown reliable design code and unreliable design procedure for normal and high strength steel, respectively. Laim et al. [16] conducted a series of bending tests and also finite element modellings on flexural behaviour of cold-formed steel beams. The authors reported that the dominant failure mode was distortional buckling. Folded-flange sections were developed to present the best performance under bending investigation compared to other typical and industrial sections (the flexural capacity increased by up to 50%), and using partial reinforcing significantly increased the beam strength against the lateral-torsion buckling [17,18]. Muftah et al. [19] performed a series of four-point flexural tests on bolted built-up cold-formed steel beams while using bolts and nuts system. According to the reported conclusions, when the loads were applied on the webs, the flexural behaviour of the beams was dependent just on bolt distances. Huang et al. [20] proposed a novel solution to the distortional buckling moment for stiffened CFS beams based on the minimum potential energy rules and using web and flange stiffeners. The presence of flange stiffeners enhanced the bearing capacity and increased the distortional buckling moment [21]. The presence of slots affected both the shear rigidity and distortional buckling load and the web stiffeners improved the flexural behavior [22].

Following the literature, perforated CFS beams subjected to different bending scenarios should be able to deal with different buckling modes [23]. There is almost no simple way to address this significant concern. Hence, this study proposed a simple and low-cost reinforcing system for CFS uprights consisting of a bolt, nut and spacer. A series of four-point bending tests were performed on the specific stiffened perforated beams to measure the buckling-resistant moment of an upright section about its major and minor axes and to evaluate its improvement by proposed reinforcement. A total of eighteen monotonic tests were conducted to determine both the flexural capacity and failure modes of the reinforced sections, which consisted of uprights with 1.6 mm thickness strengthened by bolt and spacer systems. Finite element (FE) analysis was also performed by ABAQUS program and was verified by the experimental results. The comparison of the parametric study and test study showed both outstanding accuracy for the experimental results, and the proficiency of the proposed reinforcing system.

2. Reinforcement Method

Three principal buckling modes for upright sections observed during the flexural test are distortional, flexural and flexural-torsional. However, the distortional buckling is the governing mode in the design of uprights, where excessive deformation occurs about a weaker principal axis.

The typical upright frame consists of a regular pattern of perforations which can be placed on both the web and the lips. Web perforations are used for fast interconnection between beams and uprights, while lip perforations allow the connection of the brace components to uprights. The

location of perforations which are not in use in the section lip can also be used to partially close off the section. Therefore, in this study, stiffeners comprised of fasteners, nuts and spacers were used at the location of perforations to connect the lips of the open sections and to improve the moment capacity of the system. These stiffeners are commonly used to attach the brace to uprights; hence, no further design is required for these connectors.

Time-consuming and costly stiffening methods, such as plate stiffeners and partially closing the sections, are not practical for upright frames already in use. Preliminary numerical analyses were also performed in order to check the feasibility and capability of the proposed reinforcing method, and it was found that this approach can increase the load-bearing capacity of standard uprights. The strengthening method proposed in this study is a handy and cost-effective approach that can be used for all racking systems, especially those which are currently in use in storage locations. This approach can be employed for all CFS open sections as well [24,25]. The reinforcement arrangement consisted of a bolt, nut and double spacer, where the spacer was the transverse element made up of the plastic material commonly used for bracing of racking by attaching to the lips of the section. The reinforcing details are demonstrated in Figure 1.

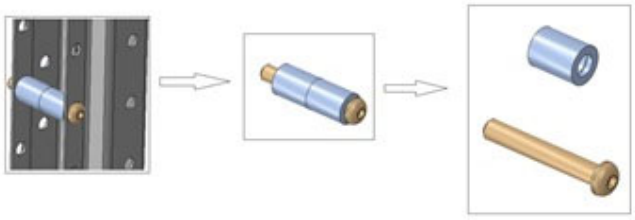

(**A**)

(**B**)

Figure 1. Reinforcement by bolts and spacers: (**A**) Schematic view; (**B**) Along the upright.

3. Experimental Campaign

The experimental investigation was performed at the structural laboratory of Western Sydney University in order to determine the moment capacity of an upright section about its major and minor axes of bending and its improvement by different patterns of reinforcement by adding bolts, spacers and partially closing the sections. The experimental test details are discussed in the next section.

3.1. Test Specimens

Eighteen specimens consisting of nine single-upright and nine bending frames were prepared for testing. The bending frames including two upright columns attached by diagonal bracing were constructed from commercially available rack sections, and the ends of the frame were constrained by back-to-back bracing to avoid twisting. Specimens were produced in two groups, with or without reinforcements. The specimen specifications are tabulated in Table 1. Figure 2 indicates the section and the perforation details as well as the frame configurations.

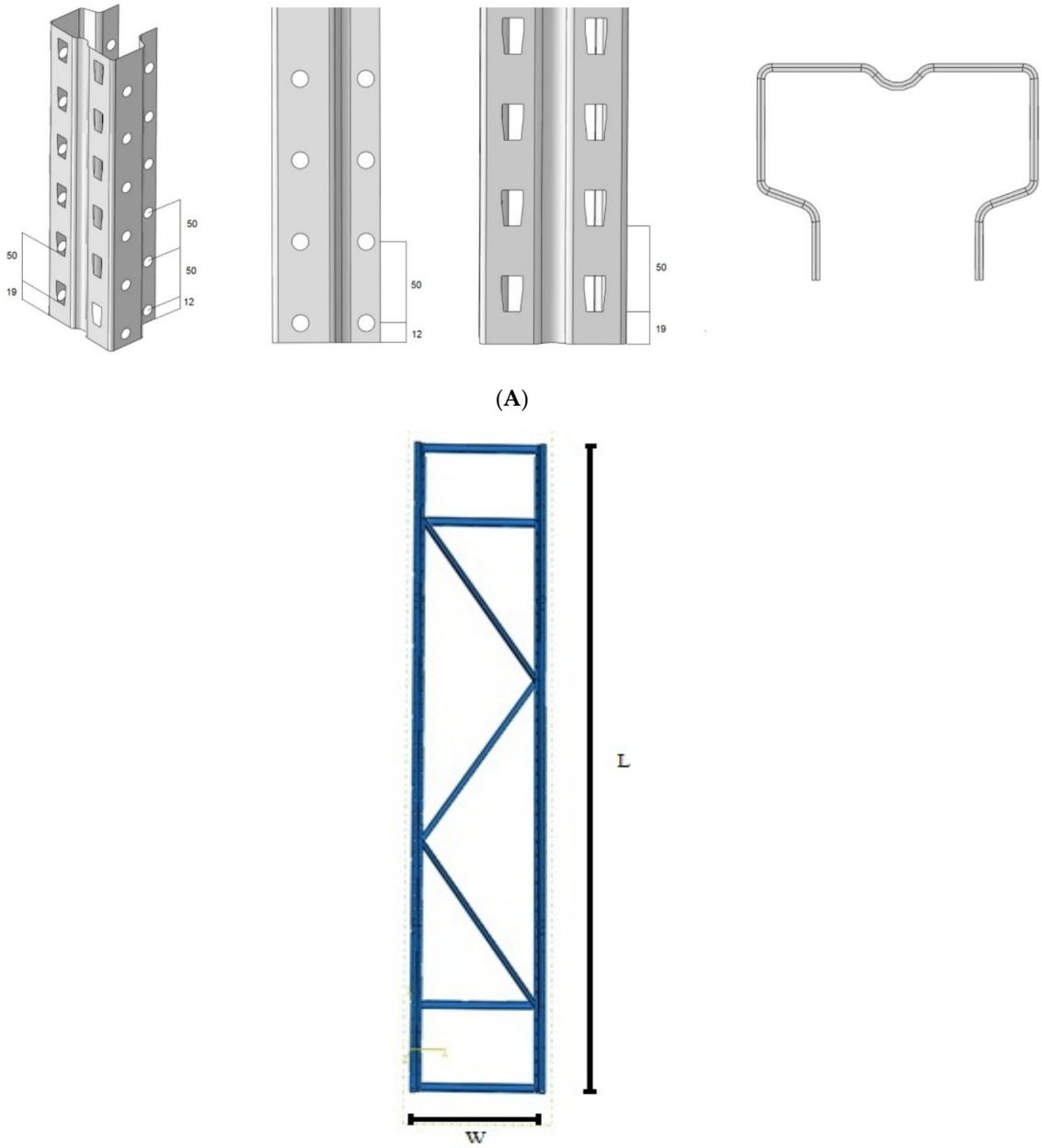

(**A**)

(**B**)

Figure 2. Configuration of the details: (**A**) Upright configuration; (**B**) Frame configuration.

Table 1. Specimen configurations.

Specimen Type	Geometry (mm)				Reinforcement	Loading Direction	
	* Length	** Thickness	*** Width	**** S_p		Major Axis	Minor Axis
SMIM	2400	1.6	600	-	No		•
SMIM				-	No		•
SMIM				-	No		•
SMJM				-	No	•	
SMJM				-	No	•	
SMJM				-	No	•	
200RMIM				200	Yes		•
200RMIM				200	Yes		•
200RMIM				200	Yes		•
200RMJM				200	Yes	•	
200RMJM				200	Yes	•	
200RMJM				200	Yes	•	
300RMIM				300	Yes		•
300RMIM				300	Yes		•
300RMIM				300	Yes		•
300RMJM				300	Yes	•	
300RMJM				300	Yes	•	
300RMJM				300	Yes	•	

* Length = upright length. ** Thickness = upright thickness. *** Width = frame width (distance between two upright). **** Sp = distance between reinforcement bolts (reinforcement space).

The convention used to designate the specimens is explained in Figure 3. The SMIM and SMJM specimens were manufactured without reinforcements, and their flexural behaviour was investigated during the monotonic test. Their loading direction was carried out on the minor and major axes, respectively. The 200RMIM and 200RMJM specimens were produced with reinforcements placed at 200 mm spacing along the upright length and were investigated about their minor and major axes respectively. The 300RMIM and 300RMJM specimens were developed according to the previous patterns except that their reinforcement spaces were 300 mm.

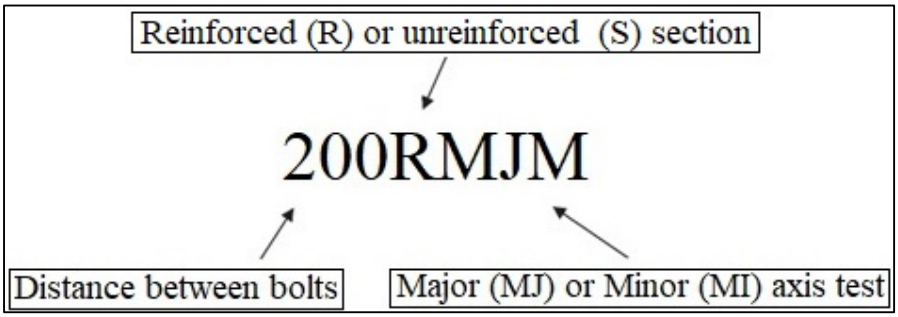

Figure 3. Designation of specimens.

3.2. Material Properties

The tensile coupon test is essential to identify the actual material properties of the test specimen. Three coupons from the upright flanges with no perforations were prepared for the coupon test. The CFS channel section was cleaned, cleared and cut into coupon-shaped flexural specimens. The tensile test was conducted according to AS4600 procedures [26].

The tensile test results were used for developing finite element models that are presented later in this paper. An MTS Sintech testing machine (TestResources Inc., Shakopee, MN, USA) with 300 kN capacity and a rate of 0.01 mm/s was used for the coupon tests. Figure 4 shows the stress-strain

curves for 1.6 mm thickness sections. The mean values of the ultimate tensile strength (σ_u), and yield stress (σ_y) and elongation are presented in Table 2.

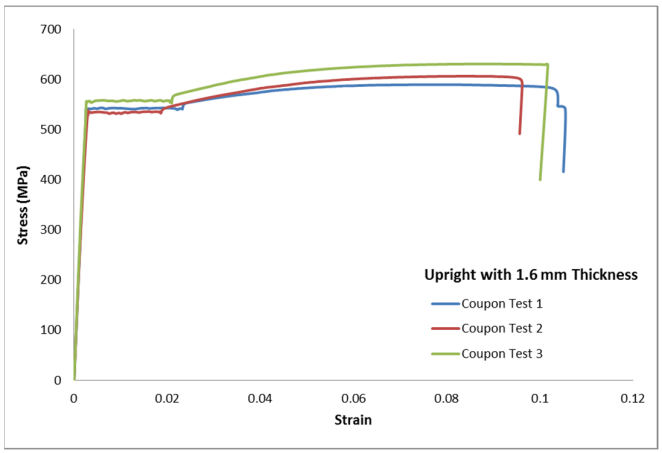

Figure 4. Stress-strain diagram for 1.6 mm thickness specimen.

Table 2. Material properties of the upright section.

Section Type	Yield Stress, σ_y (MPa)	Ultimate Stress, σ_u (MPa)	Elongation (%)
Upright with 1.6 mm thickness (Test 1)	561	578	10.3
Upright with 1.6 mm thickness (Test 2)	557	585	9.6
Upright with 1.6 mm thickness (Test 3)	571	610	10.1
Average	563	591	10

3.3. Test Set-up

The purpose of the four-point bending test is to determine the flexural moment capacity of an upright section about its major and minor axes of bending and its improvement by different patterns of reinforcement by adding bolts, spacers and partially closing its sections. The flexural test was carried out to simulate the pure bending using a four-point bending test according to AS 4084:2012 [27] Section 7.3.4: Bending tests on upright sections (Figure 5).

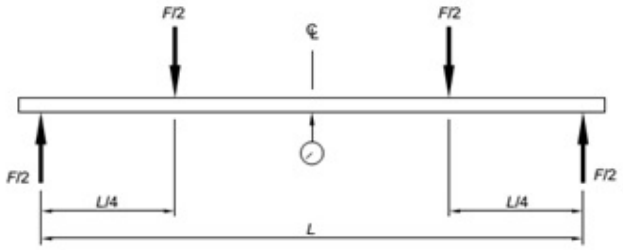

Figure 5. Typical schematic four-point bending test.

In the test section, the actuator was placed on two steel I-beams, and the I-beams were settled on the steel girders to transmit the applied force on spherical rollers. The steel spherical rollers were placed on the test specimen to facilitate the movement of the specimen not only to show the potential deformations but to simulate the real condition for pure bending. The rollers were placed on two

perforated steel plates. The details and the schematic views of the minor axis test set-up are shown in Figure 6.

(**A**)

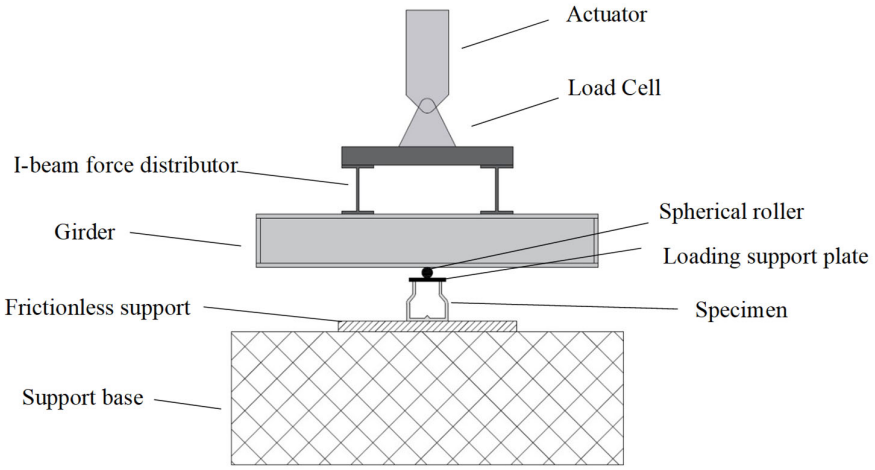

(**B**)

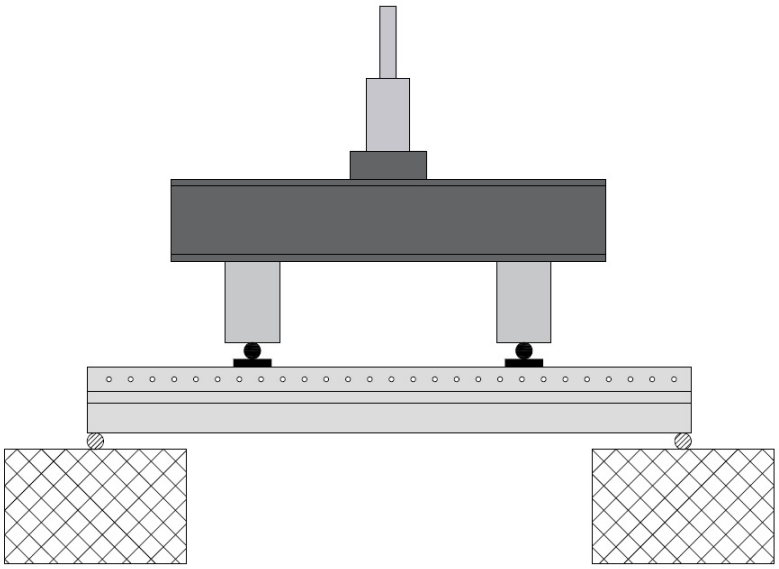

(**C**)

Figure 6. Minor axis test set-up details: (**A**) Test specimen; (**B**) schematic front view; (**C**) schematic side view.

The major axis test was designed to measure both the bending strength of the upright about the major axis and the buckling modes. Because of the potential distortion and torsional displacement of the section, as shown in Figure 7 the designed major axis test specimens contained two studs as a single frame so that the specimens would demonstrate appropriate flexural behaviour during the monotonic loading. Also, the actuator was placed on two steel I-beams, and the I-beams were settled on two steel girders which transmitted the force onto the roller supports. Put et al. [28] performed a series of eccentrically and concentrically loading on the channel steel upright connections. The more eccentricity increases, the more beam strength decreases. Therefore, for the major axis tests, the rollers settled on four perforated steel angles attached to the web of the channel by four fasteners designed to exert the load to the shear center of the profile section. That being the case, the spherical rollers and loading angles were designed to let any possible displacement, especially the distortional buckling, happen. Also, the specimen was free to twist on the frictionless supports. By this means, this test arrangement permits buckling modes to occur similar to the real modes developed by the upright in its normal usage. Three tests for each type of the specimens and about each axis were carried out including unreinforced profiles and reinforced ones.

(**A**)

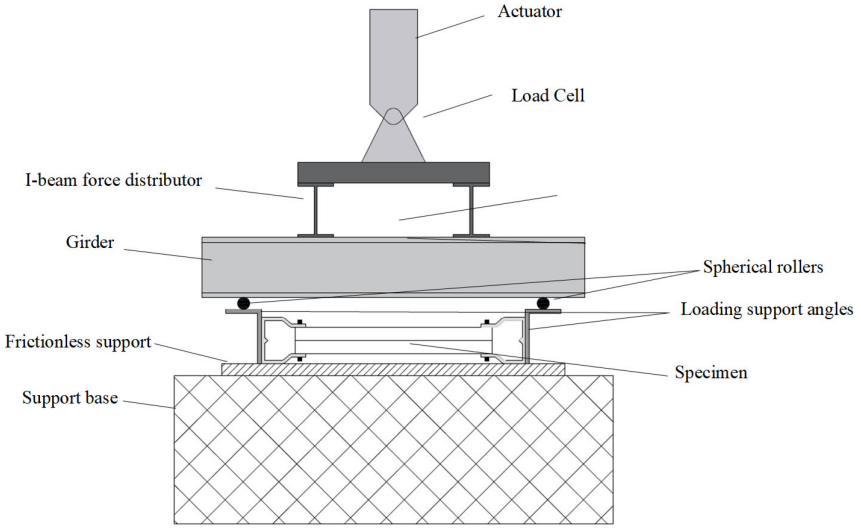

(**B**)

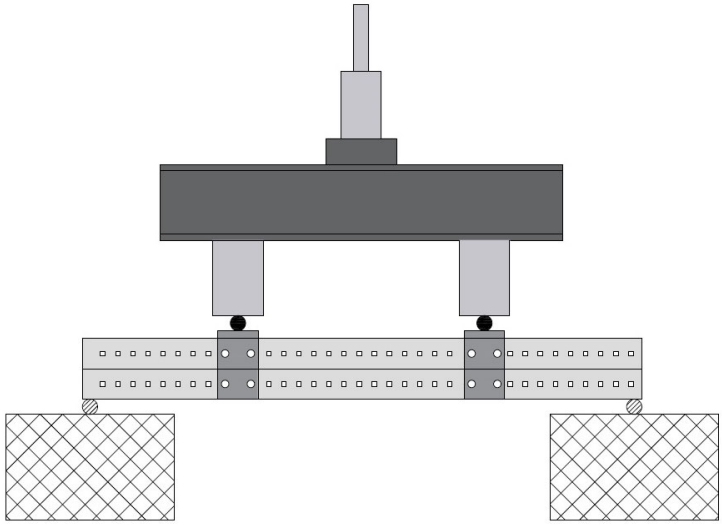

(**C**)

Figure 7. Major axis test set-up details: (**A**) Test specimen; (**B**) schematic front view; (**C**) schematic side view.

Although the roller supports were designed to be at the shear centre of the uprights and act delicately in case of load transfer, the preliminary tests faced the problem of local crushing and crippling in the vicinity of the loading angles and rollers. This issue was addressed by using reinforcement just underneath the supports, as shown in Figure 8.

(**A**) (**B**)

Figure 8. Crippling of load points: (**A**) Typical crippling at flanges; (**B**) Specific crippling reinforcement.

In total, 18 monotonic tests (single directional force) were conducted during the investigation based on AS 4084: 2012, Section 7.3.4: Bending tests on upright sections [27] to determine the failure moment and mode of the pallet racking's uprights (Figure 9).

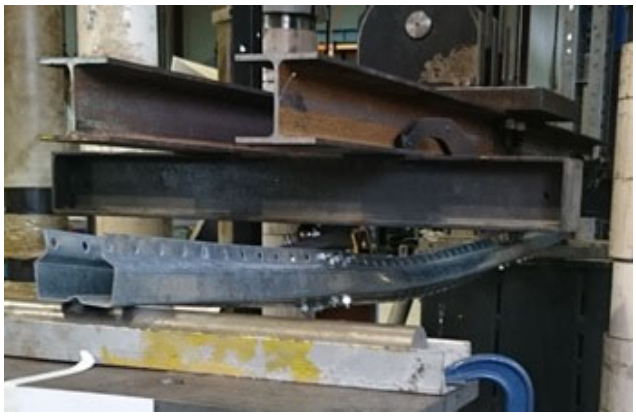

(**A**)

(**B**)

Figure 9. Test set-up: (**A**) minor axis test, (**B**) major axis test.

3.4. Data Acquisition and Instrumentation

The experiments were conducted using a Universal Testing Machine, Instron 8506 (Instron, Norwood, MA, USA) with 3000 kN capacity. The loading rate of 0.5 mm/min was applied to the specimens. The reading of the forces was measured by the load cell, whereas the deflection of the uprights was measured by linear variable differential transformers (LVDTs). The data was collected via data logger and sent to the computer then processed with Microsoft Excel. The data was measured at a frequency of 2 Hz, which means every 0.5 s.

4. Test Results and Discussion

Eighteen specimens with 2400 mm length and 1.6 mm thickness were tested in three reinforcement compositions: without reinforcement, and with reinforcements at 200 mm and 300 mm. The tests aimed to investigate the reinforcement effect on flexural performance. The tests were designed to acquire both the flexural capacity and the failure modes during the loading process.

The flexural moment capacity for each specimen was recorded and due to confidentiality matters, it was normalised with respect to the normalization factor ($N_f = Z.\ \sigma_y$), where Z was the shape factor of the section, and σ_y was the yield-stress extracted by the coupon tests. On the other hand, the deflection value represents the displacement of the mid-point in each specimen recorded by LVDTs. For each specimen type, three tests were conducted to ensure the accuracy of the results for the upright flexural behaviour.

4.1. Major Axis Test

Figure 10 demonstrates the normalised bending moment versus deflection for unreinforced, 200 mm and 300 mm reinforcement types under monotonic flexural tests. The 200 mm reinforcement type provided the highest flexural strength compared to the other two types. The normalized bending moment capacity for each specimen is tabulated in Table 3. Factors responsible for some differences in the results for the same specimen types could be either typical shortcomings during the set-up adjustment or probable various initial geometric imperfections associated with the manufacturing processes.

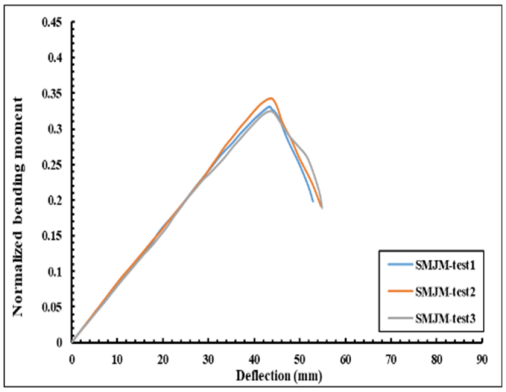

(**A**)

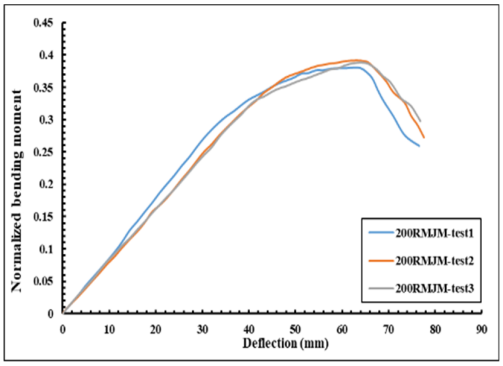

(**B**)

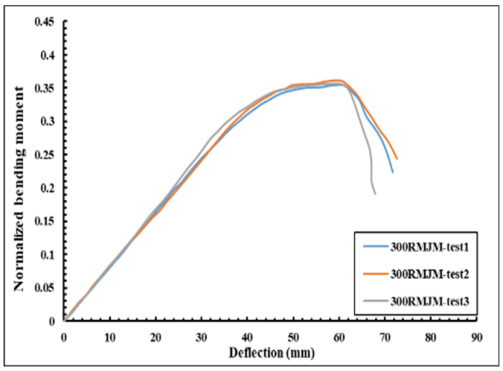

(**C**)

Figure 10. Normalized bending moment–deflection about major axis curves: (**A**) SMJM; (**B**) 200RMJM; (**C**) 300RMJM.

Table 3. The ultimate normalized bending capacity of specimens in the major axis test.

Test Specimen	Normalised Ultimate Bending moment $\left(\frac{M}{\sigma_y \times Z}\right)$
SMJM-Test1	0.330997561

SMJM-Test2	0.342394439
SMJM-Test3	0.325000724
Average	0.332797575
Standard deviation	0.008835461
200RMJM-Test1	0.379727867
200RMJM-Test2	0.391261742
200RMJM-Test3	0.388300744
Average	0.386430118
Standard deviation	0.005990158
300RMJM-Test1	0.354944611
300RMJM-Test2	0.361971684
300RMJM-Test3	0.356490403
Average	0.357802233
Standard deviation	0.003692643

Both the distortional and local buckling were observed during major axis testing of the unreinforced frames (Figure 11). According to the observations, some notches were observed along with the failure mechanism at the local buckling zones.

(**A**)

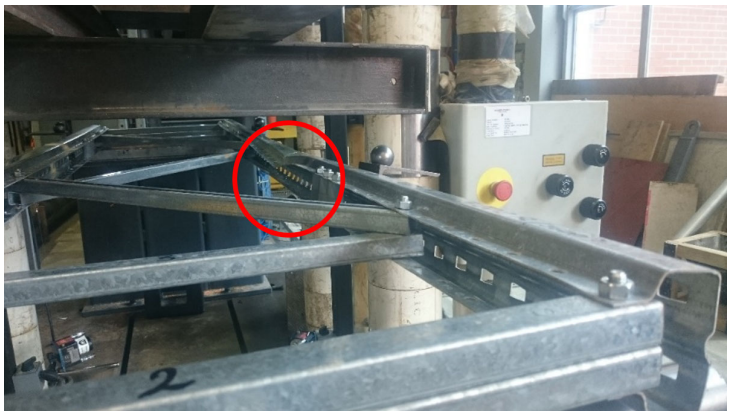

(**B**)

(**C**)

Figure 11. The observed failure mode for unreinforced specimens during the major axis test: (**A**) SMJM-test1; (**B**) SMJM-test2; (**C**) SMJM-test3.

When the reinforced specimens with 200 mm reinforcing pitch were subjected to the monotonic displacement control test on the major axis, local buckling, as well as a combination of both local and distortional buckling, occurred during the experiments. The yielding notches were also observed as crippling signs in some areas (Figure 12).

(**A**)

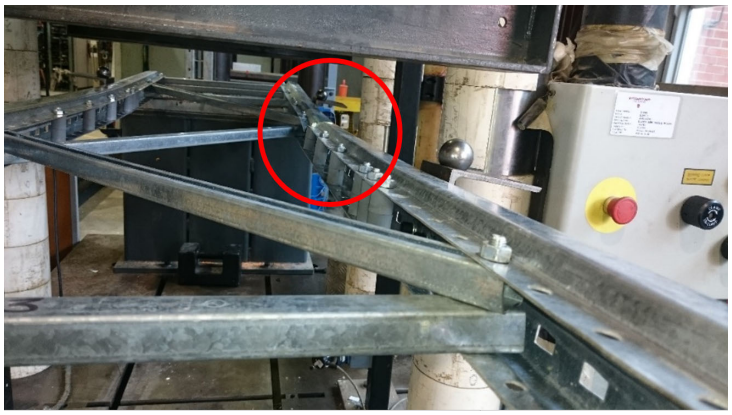

(**B**)

(**C**)

Figure 12. The observed failure mode for reinforced specimens with 200 mm reinforcing pitch during the major axis test: (**A**) 200RMJM-test1; (**B**) 200RMJM-test2; (**C**) 200RMJM-test3.

Following the experimental investigation, the reinforced specimens with 300 mm reinforcing pitch were subjected to the major axis displacement control monotonic test (Figure 13). The governing failure mode at these tests was also the distortional and local buckling.

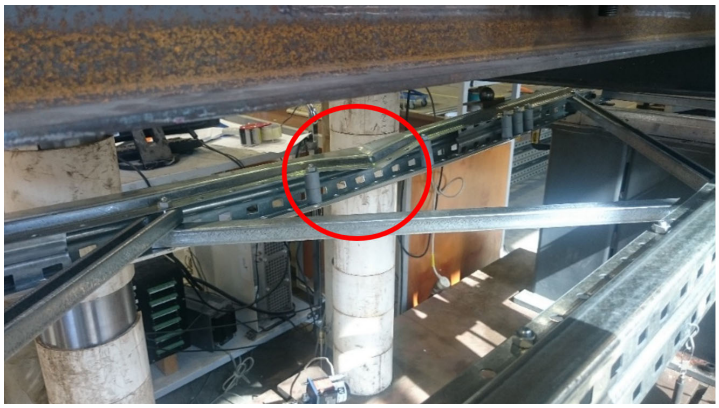

(**A**)

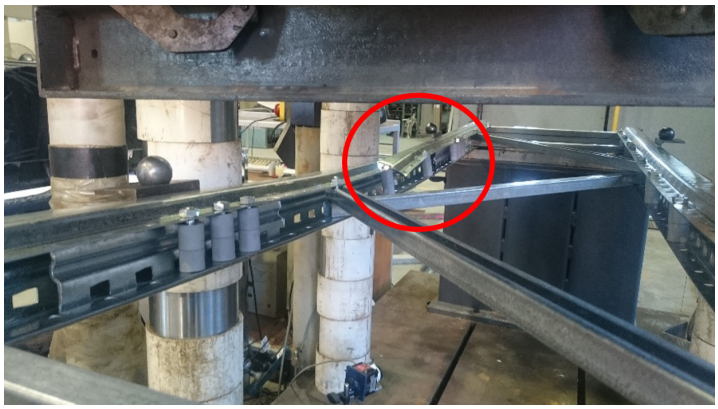

(**B**)

(**C**)

Figure 13. The observed failure modes for reinforced specimens with 300 mm reinforcing space during the major axis test: (**A**) 300RMJM-test1; (**B**) 300RMJM-test2; (**C**) 300RMJM-test3.

To compare the flexural behaviour of the uprights, the mean curves shown in Figure 14 presented the effect of reinforcements with respect to the average normalized bending. According to Figure 14, it is clear that using reinforcements improves both the ultimate capacity and deflection of the specimens; however, this improvement has been enhanced by using the 200 mm reinforcement type. Figure 14 shows the 200 mm pitch improved the flexural behaviour of the uprights and also increased the bending capacity.

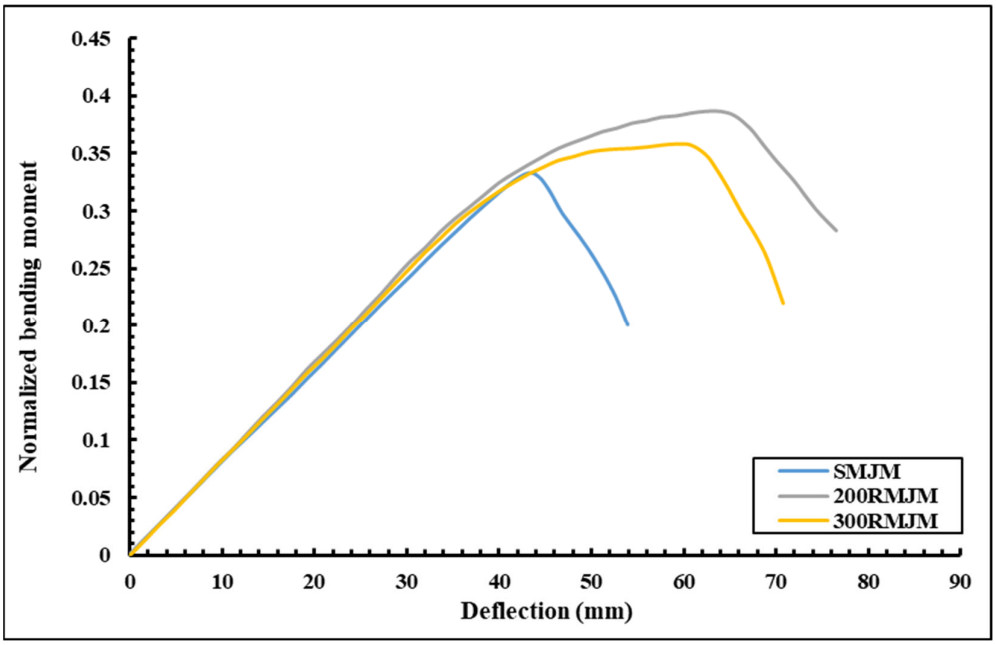

Figure 14. The normalized major axis test average curves.

The reported experimental results show the effectiveness of the presence of reinforcements. Figure 15 compares the different reinforcement types used. In Figure 15, the 200 mm reinforcement type showed 13.8% and 7.35% enhanced capacity compared to the non-reinforced and 300 mm reinforcement type, respectively. The 300 mm type showed 6.97% improvement in bending capacity compared to the unreinforced specimen. Typically, the failure modes which were observed in the major axis experimental tests were local and distortional bucklings.

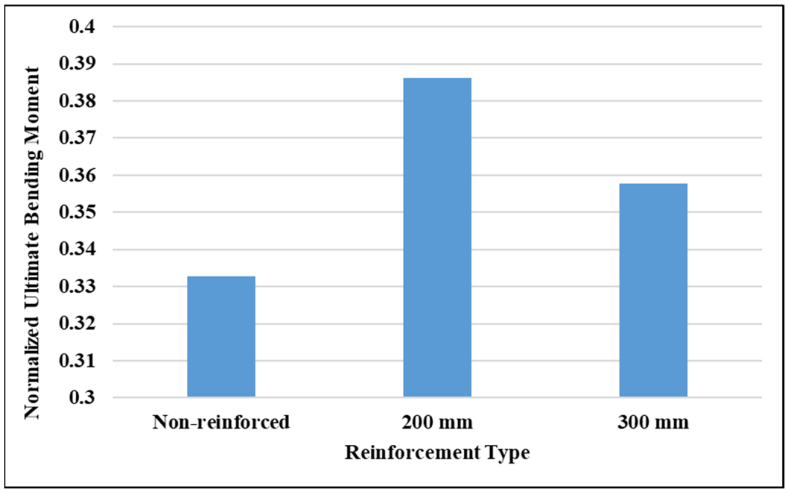

Figure 15. The ultimate normalized moment for major axis test with respect to the reinforcement type.

4.2. Minor Axis Test

Figure 16 presents the normalized bending moment–deflection curves for unreinforced, 200 mm and 300 mm reinforcement types where the flexural behaviour of the specimens under minor axis tests has been reported.

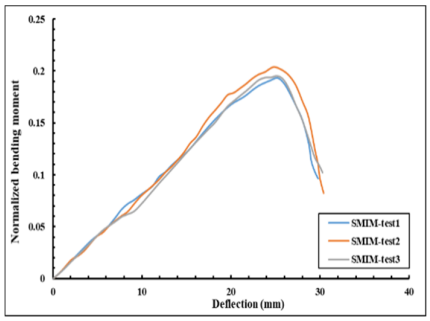

(**A**)

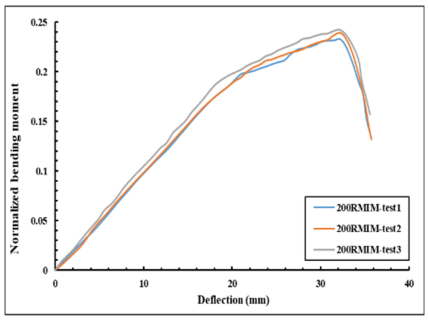

(**B**)

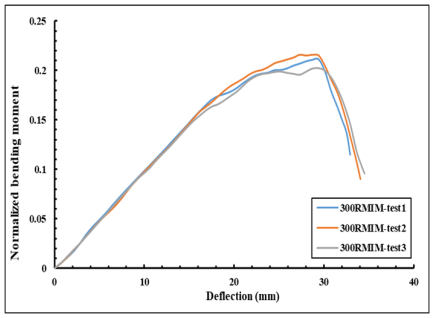

(**C**)

Figure 16. Normalized bending moment–deflection about minor axis test curves: (**A**) SMIM; (**B**) 200RMIM; (**C**) 300RMIM.

The 200 mm reinforcement type captured the best flexural performance compared to the other two types. The normalized bending capacity for each specimen is also tabulated in Table 4.

Table 4. The ultimate normalized bending capacity of specimens in the minor axis tests.

Test Specimen	Normalized Ultimate Bending Moment $(\frac{M}{\sigma_y \times Z})$
SMIM-Test1	0.193595703
SMIM-Test2	0.203694478
SMIM-Test3	0.195419898
Average	0.197570026
Standard deviation	0.005381785
200RMIM-Test1	0.232982073
200RMIM-Test2	0.239285101
200RMIM-Test3	0.242392113
Average	0.238219762
Standard deviation	0.004794624
300RMIM-Test1	0.211013767
300RMIM-Test2	0.21581945
300RMIM-Test3	0.202362802
Average	0.209732006
Standard deviation	0.006819276

Figure 17 represents the minor axis test for the single unreinforced uprights, showing the uprights' distortional buckling in the tests.

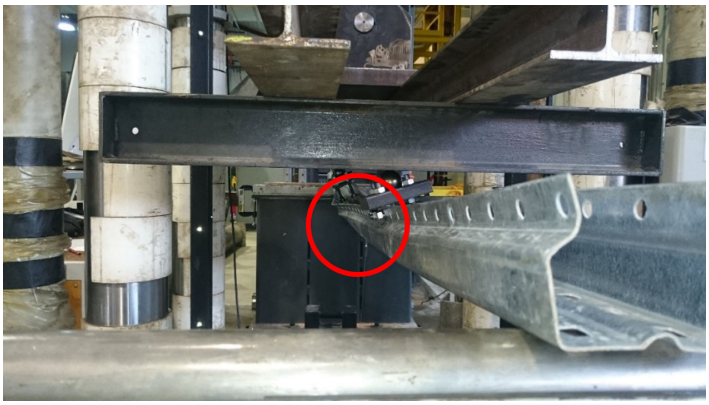

(**A**)

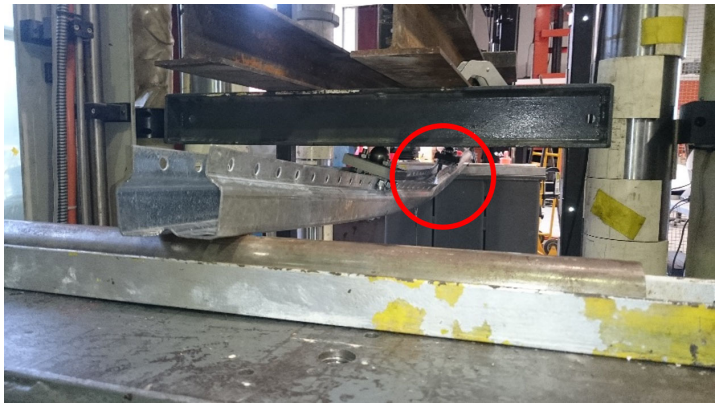

(**B**)

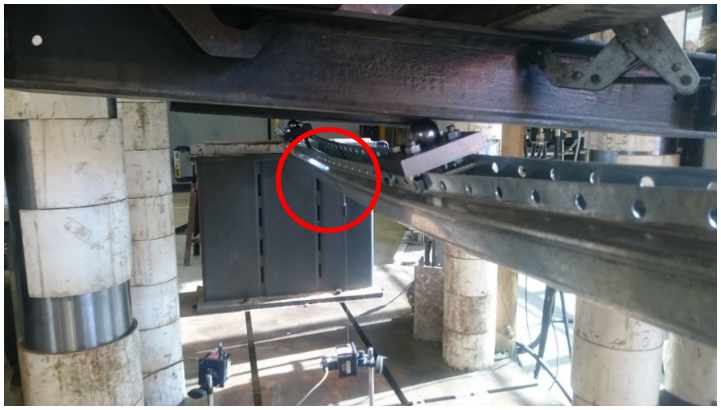

(**C**)

Figure 17. The observed failure mode for unreinforced specimens during the minor axis test: (**A**) SMIM-test1; (**B**) SMIM-test2; (**C**) SMIM-test3.

The reinforced specimens with 200 mm reinforcing space were subjected to the minor axis tests as shown in Figure 18. Based on the test observations, the mid-span deflections were much higher than the unreinforced specimens. The reinforced specimens exhibited no sudden torsion or twisting, but the bending capacity was enhanced significantly in the 200 mm reinforcing type.

(**A**)

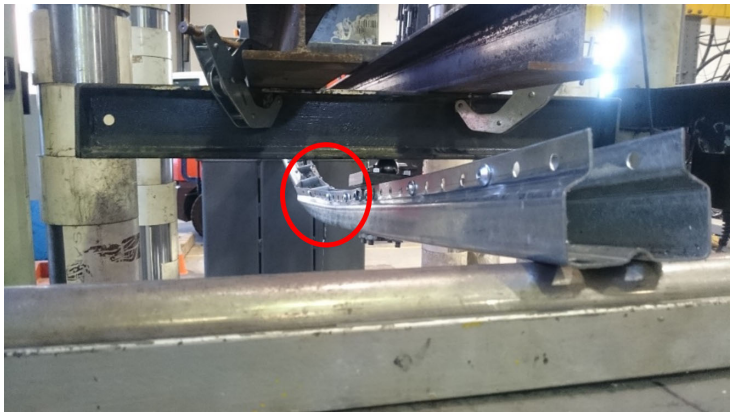

(**B**)

(**C**)

Figure 18. The observed failure mode for reinforced specimens with 200 mm reinforcing pitch during the minor axis test: (**A**) 200RMIM-test1; (**B**) 200RMIM-test2; (**C**) 200RMIM-test3.

The minor axis test was performed on 300 mm reinforced specimens. Observations proved that increasing the reinforcing space decreases the section flexural capacity compared to the 200 mm specimens as well as the ultimate deflection of the sections at the time of failure (Figure 19).

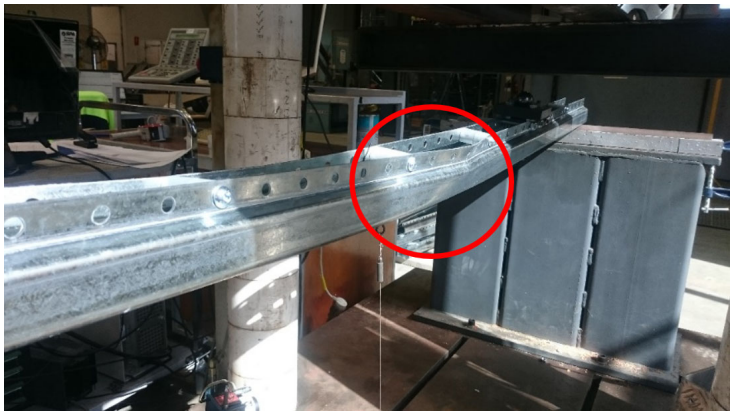

(**A**)

(**B**)

(**C**)

Figure 19. The observed failure mode for reinforced specimens with 300 mm reinforcing pitch during the minor axis test: (**A**) 300RMIM-test1; (**B**) 300RMIM-test2; (**C**) 300RMIM-test3.

The normalized mean bending moment versus deflection curves demonstrated in Figure 20 represent the effects of the reinforcements in the minor axis tests. According to Figure 20, non-reinforced specimens had lower bending capacity. However, 200 and 300 mm reinforcement types presented improved behaviour, especially in the ultimate capacity and deflection.

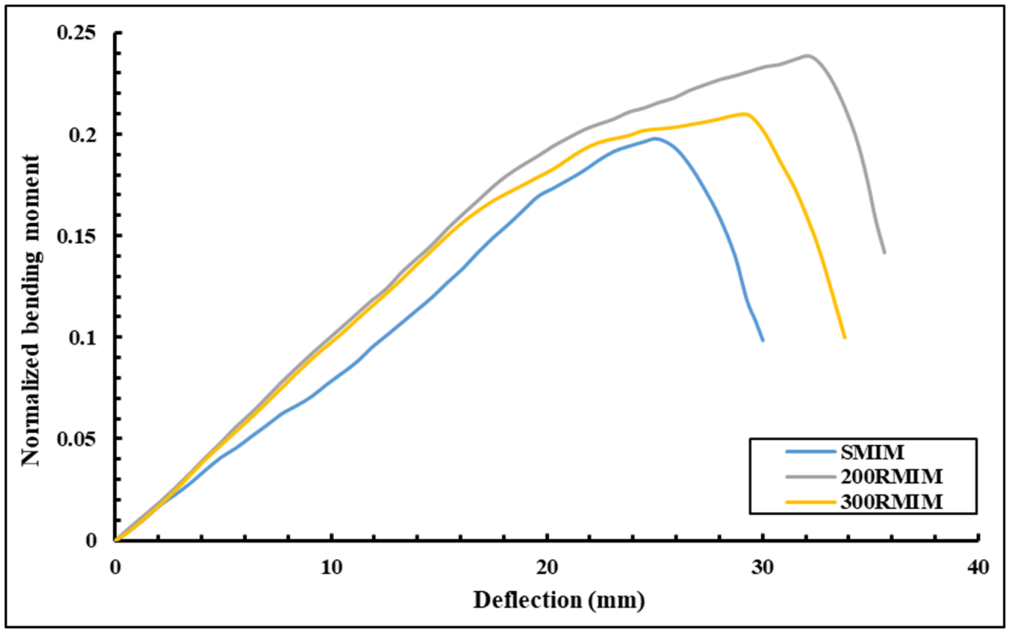

Figure 20. The normalized minor axis average curves.

Figure 21 presents the influence of performed reinforcement types. The 200 mm reinforcement type resulted in 12% and 17% improvement in ultimate bending capacity compared to the 300 mm reinforcement and non-reinforced types, respectively. The 300 mm type showed a 5.5% improvement in ultimate bending capacity compared to the non-reinforced specimen.

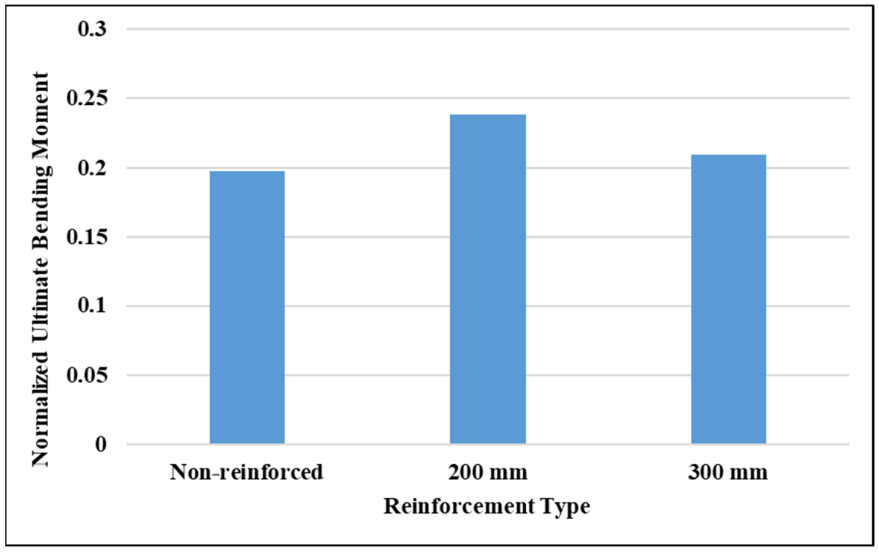

Figure 21. The ultimate normalized moment for the minor axis test by reinforcement type.

4.3. Remarks on the Results

Based on the results of both experimental and numerical investigations, the governing failure mechanisms can be categorized into two main types: buckling or crippling. First of all, local and distortional bucklings happened in almost every unreinforced specimen's major axis test. These failure mechanisms were located near the weakest zone of the beam, which was typically the mid-span of the specimens. Local bucklings were mostly observed in 200 mm type reinforced specimens,

but the presence of condense reinforcing was acting as the constraining factor. As the reinforcing pitch was enlarged, the distortional buckling became the dominant failure mode as observed in the 300 mm reinforcing types. The change in the section's half-wavelength resulted in the change of buckling mode and failure load. Reducing the half-wavelength by decreasing the reinforcement pitch increases the distortional buckling capacity as well as changing the mode from distortional to local–distortional in some cases.

Secondly, in the case of crippling as another factor of failure, the unreinforced specimens failed due to this factor, especially in the major axis tests. The 200 mm and 300 mm reinforcing types also failed through the crippling mechanism; however, the ultimate load of crippling was different from the unreinforced specimens. The crippling failure mechanism was initiated by a yielding notch which was exhibited on the flange. Then, due to the represented notch, the section became weak at that specific zone. Finally, this shortcoming led to the crippling and the frame collapsed.

Regarding the presented results, the reinforced frames and single-uprights showed a much better flexural performance in both the major and minor axes monotonic tests, especially the ones with 200 mm reinforcements. Furthermore, the specific reinforcements increased the section stiffness, and strengthened the uprights, especially where the uprights tend to deform or initiate buckling failure. For a better understanding, the observed buckling failure modes are demonstrated in the following sections using FE models.

5. Finite Element Models Arrangement

Different techniques are available for data validations and predictions such as artificial neural networks [29–34], FE method [1,35,36], and finite strip method [37,38]. The FE method, which is generally carried out by FE programs such as ABAQUS and ANSYS, was performed in the current study as a reliable technique for empirical data validation and response prediction. Two different FE models were used in order to simulate the experimental results of reinforcement spacing, including 200 mm, 300 mm, and without reinforcement, on the flexural strength of the upright frames about either major or minor axes. Two different arrangements were considered:

- Bending frame: The frame was modelled to simulate the major axis test, and other parts of the set-up were simulated throughout boundary condition and interaction descriptions.
- Single beam: The beam was modelled to simulate the minor axis test, and the other components of the test were simulated using appropriate stiffeners and boundary conditions.

Figure 22 (A) shows the overall arrangement for the bending frame model and (B) shows the same arrangement for single-uprights. The software ABAQUS/CAE v.12.1 was used to model the presented test specimens. The FE models were adjusted to replicate the tests.

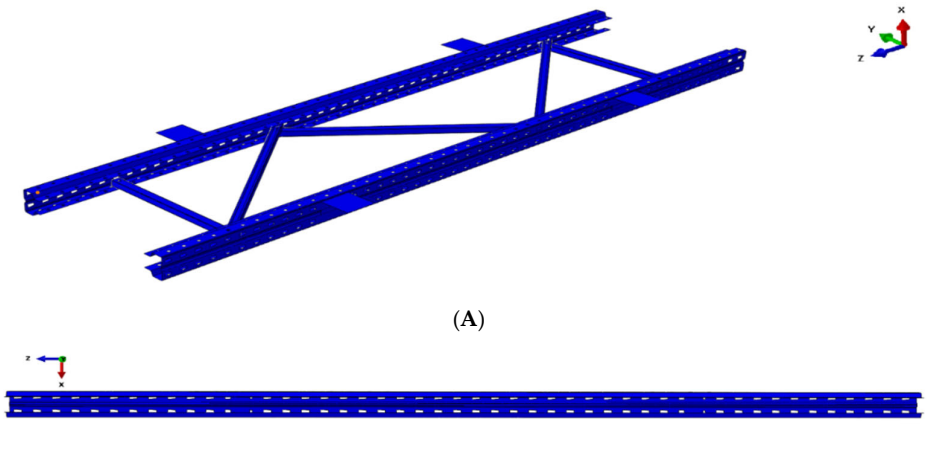

(**A**)

(**B**)

Figure 22. The finite element model arrangement: (**A**) major axis; (**B**) minor axis.

5.1. Element Type, Mesh Size and Material Model

Both models were simulated using four-node shell element S4R available in ABAQUS [1]. This element is a thin, shear flexible, isometric quadrilateral shell with four nodes and five degrees of freedom per node, using reduced integration and bilinear interpolation scheme (Figure 23).

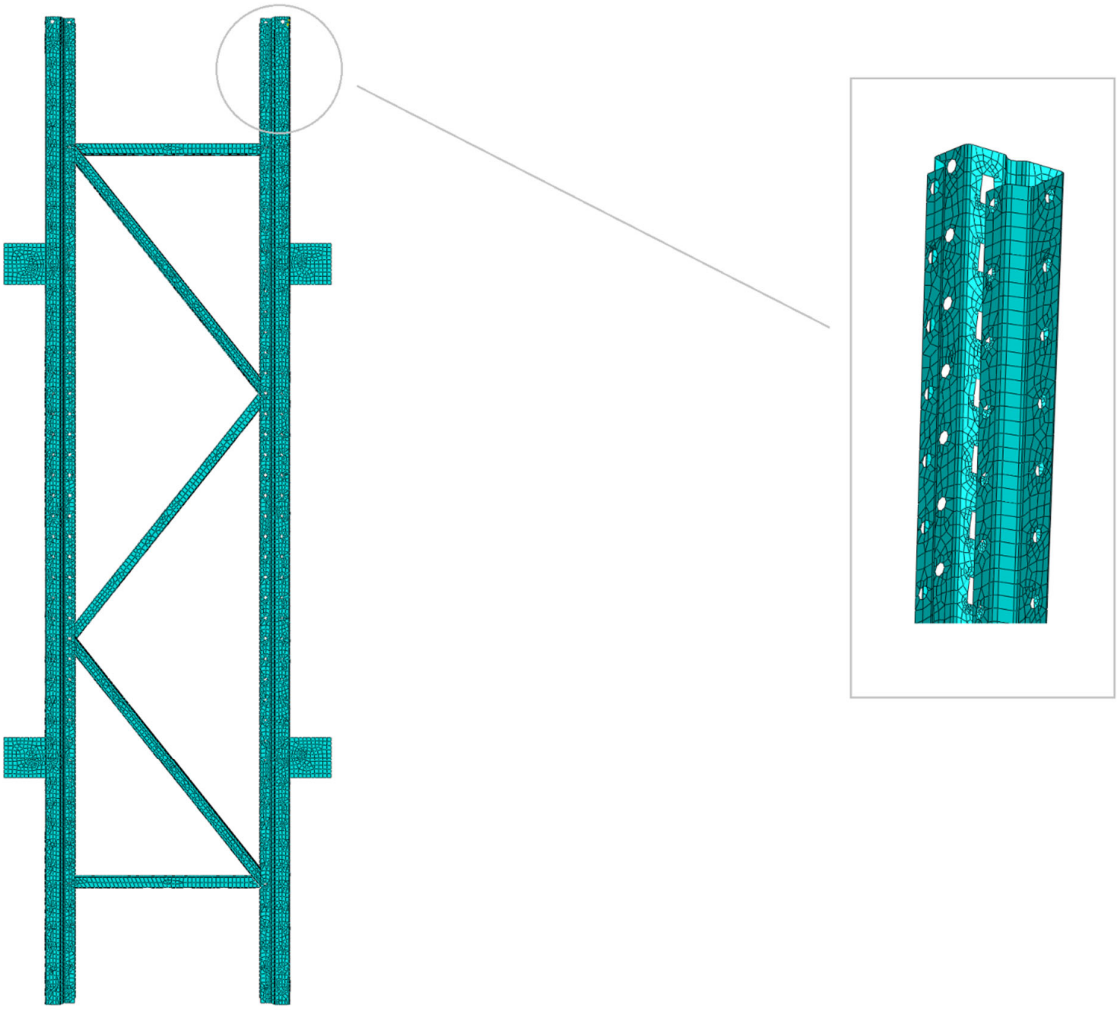

Figure 23. Typical finite element mesh of an upright section.

The stress-strain results from the tensile tests were used to model the material properties. To consider the necking phenomena in the tensile tests, the true stress-strain relationship was used for the models [39,40] with the following equations:

$$\sigma_{true} = \sigma(1 + \varepsilon) \quad (1)$$

$$\varepsilon_{true} = \ln(1 + \varepsilon) - \frac{\sigma_{true}}{E} \quad (2)$$

where σ and ε are the stresses and strains from the tensile tests. The von Mises yield criteria with isotropic hardening were also taken into account for the modelling. The modulus of elasticity was considered equal to 200 GPa and the Poisson ratio as 0.3 [1].

5.2. Connections and Interactions

For a decisive simulation, two types of interactions were defined for the FE models of the uprights subjected to loading either about the major axis or the minor axis: (a) the existing interaction of flange edges and bracing, and (b) the interaction of bracing webs at bolt connections. The surface

to surface interaction with hard contact for normal behaviour, as well as the penalty method with the friction coefficient of 0.3 for the tangential behaviour, were adopted for the model interactions [41–44]. The coupling method and beam connectors were also used to model the bolts. At each bolt location, a reference point was created at the centre of the hole where the upright flange (at the hole region) was restrained to this reference point using the coupling method [45]. The end beam restraints have also been considered as a beam using the contact pairs between the elements at two opposite sides of the sections. This type of connector constrains the axial translational degree of freedom between connecting nodes, simulating the actual bolt behaviour in the upright frame. Figure 24 indicates the existing interactions between frame elements as well as the modelling of the bolt in the upright frame.

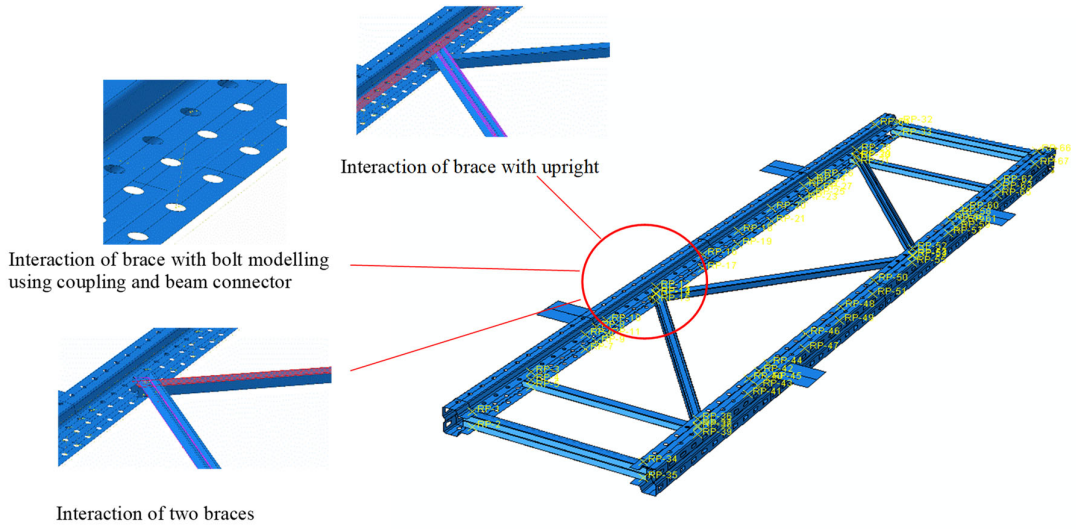

Figure 24. Interactions of the model components and bolt modelling.

5.3. Boundary Conditions and Loading

Similar to the experimental test, all boundary conditions in the FE model were also adopted in a way to represent the testing situation. The concentrated load with displacement method was applied at the shear centre of the uprights on loading support plates in the vertical direction while the translation and rotation in every direction were allowed to simulate the real testing conditions. At frictionless supports, the vertical translation was restrained to illustrate the actual support behaviour.

5.4. Validation of the Finite Element Results

According to the details in the previous sections, the FE models were generated, and the experimental simulations were carried out. The numerical results were extracted and were compared with the existing test results and failure modes to be verified. Linear regression is a powerful tool to develop predicting models for estimating the engineering properties of different materials. In this section, linear regression analyses were performed on the FE model results to help validate the results obtained from the numerical models.

5.4.1. Minor Axis

The single-upright configuration for FE modelling has been used in this section. Figure 25 compares the normalized bending moment–deflection curves of the FE model and experimental results. Figure 26 also illustrates the linear regression of the FE model mean curve with the experimental mean curve. Table 5 presents the evaluation criteria of the accuracy of the FE model predictions.

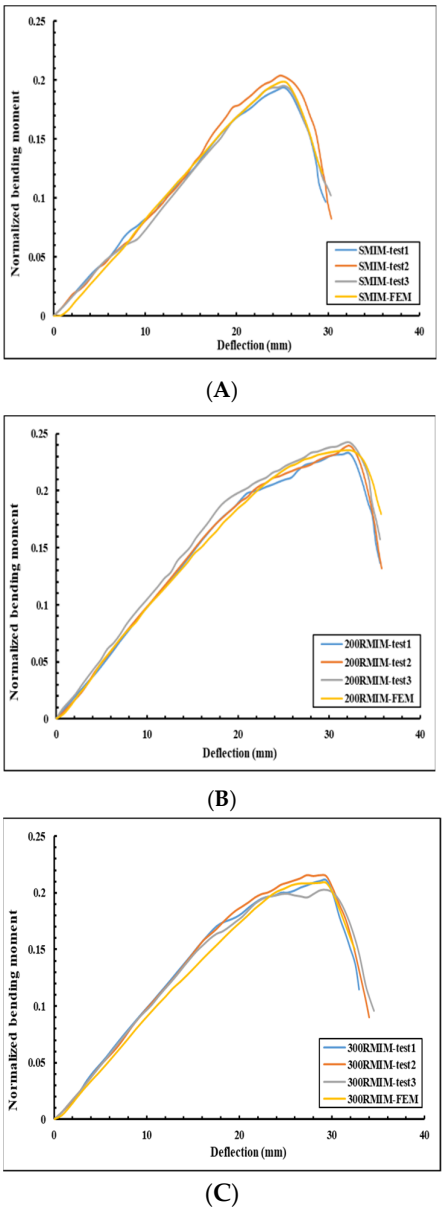

Figure 25. Finite element model and experimental curves for minor axis test set-up: (**A**) non-reinforced types; (**B**) 200 mm reinforced types; (**C**) 300 mm reinforced types.

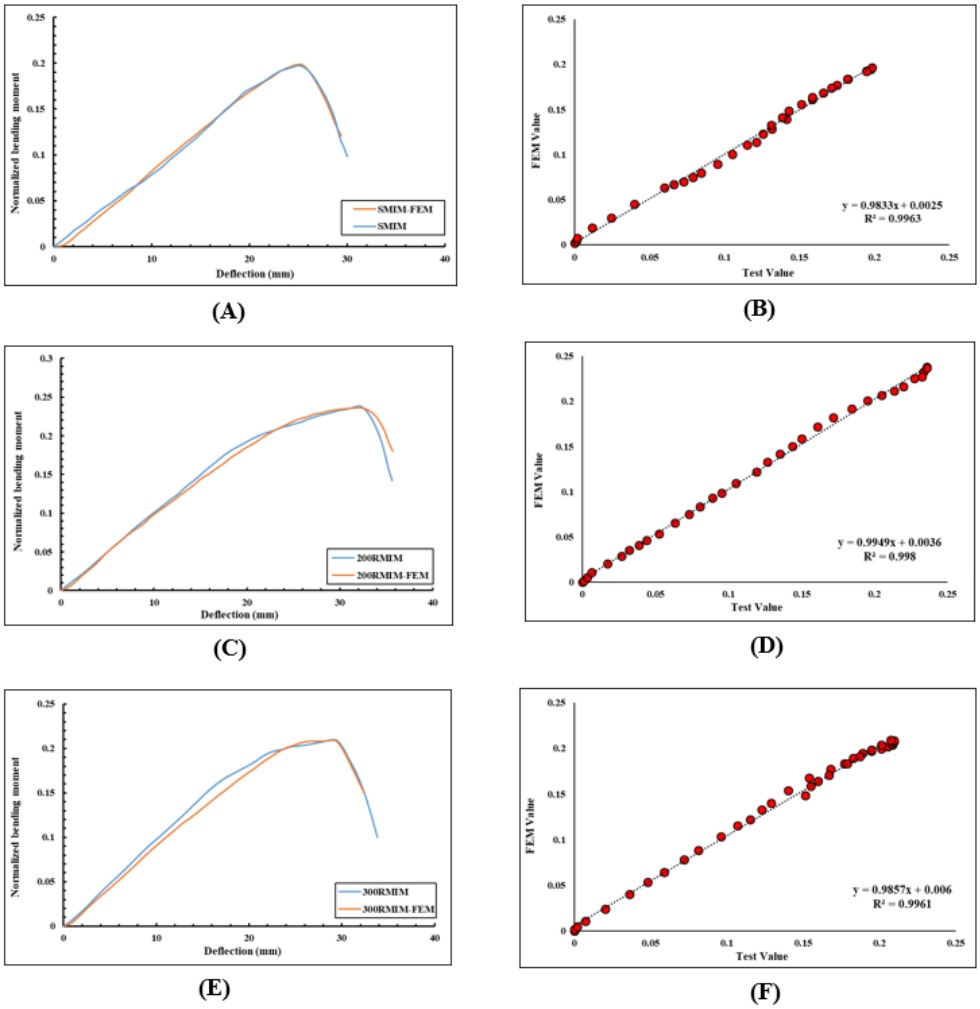

Figure 26. Comparison of finite element model against minor axis test results along with the linear regression: (**A**) and (**B**) non-reinforced model; (**C**) and (**D**) 200 mm reinforced model; (**E**) and (**F**) 300 mm reinforced model.

Table 5. Finite element model vs experimental results accuracy details in terms of evaluation criteria.

Non-reinforced model	Evaluation criteria	
	Standard deviation	0.0618701
	Pearson (r)	0.998139545
	R^2	0.9963
200 mm reinforced model	Evaluation criteria	
	Standard deviation	0.08034494
	Pearson (r)	0.993668695
	R^2	0.998
300 mm reinforced model	Evaluation criteria	
	Standard deviation	0.069798432
	Pearson (r)	0.998023512
	R^2	0.9961

According to Figure 26 and Table 5, the FE model results achieved outstanding accuracy and compatibility with the test results. In addition, Figure 27 compares the FE model failure modes of the uprights to the experimental failure modes where the developed FE model has well predicted the overall deformed shape. These uprights failed in distortional and local buckling mode.

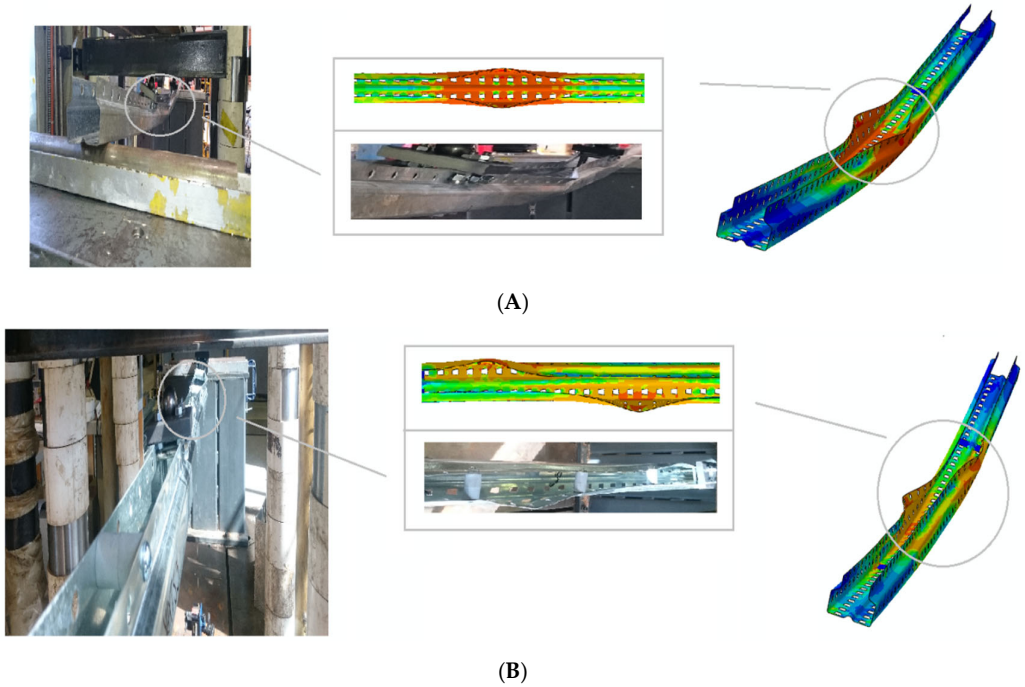

(**A**)

(**B**)

Figure 27. Comparison of failure modes: (**A**) non-reinforced upright type; (**B**) 300 mm reinforced upright type.

5.4.2. Major Axis

A bending frame arrangement was used for the numerical assessment of the upright major axis test. Figure 28 compares the normalized bending moment–deflection curves between the FE model and experimental results. Figure 29 illustrates the linear regression of the FE model mean curve with the experimental mean curve. Table 6 presents the evaluation criteria for the accuracy of the FE model predictions.

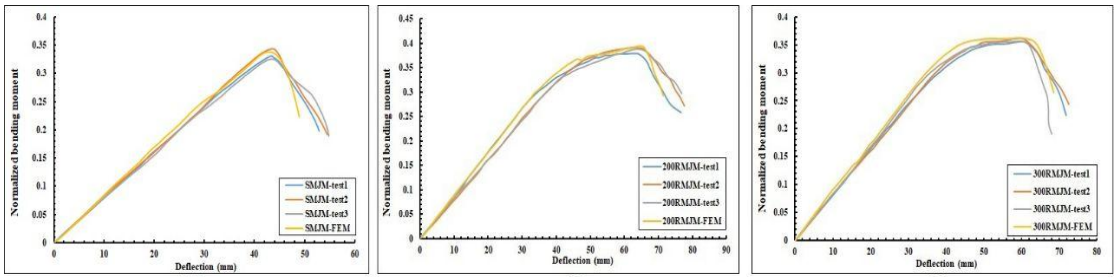

(**A**) (**B**) (**C**)

Figure 28. Finite element model and experimental curves for major axis test set-up: (**A**) non-reinforced frame types; (**B**) 200 mm reinforced frame types; (**C**) 300 mm reinforced frame types.

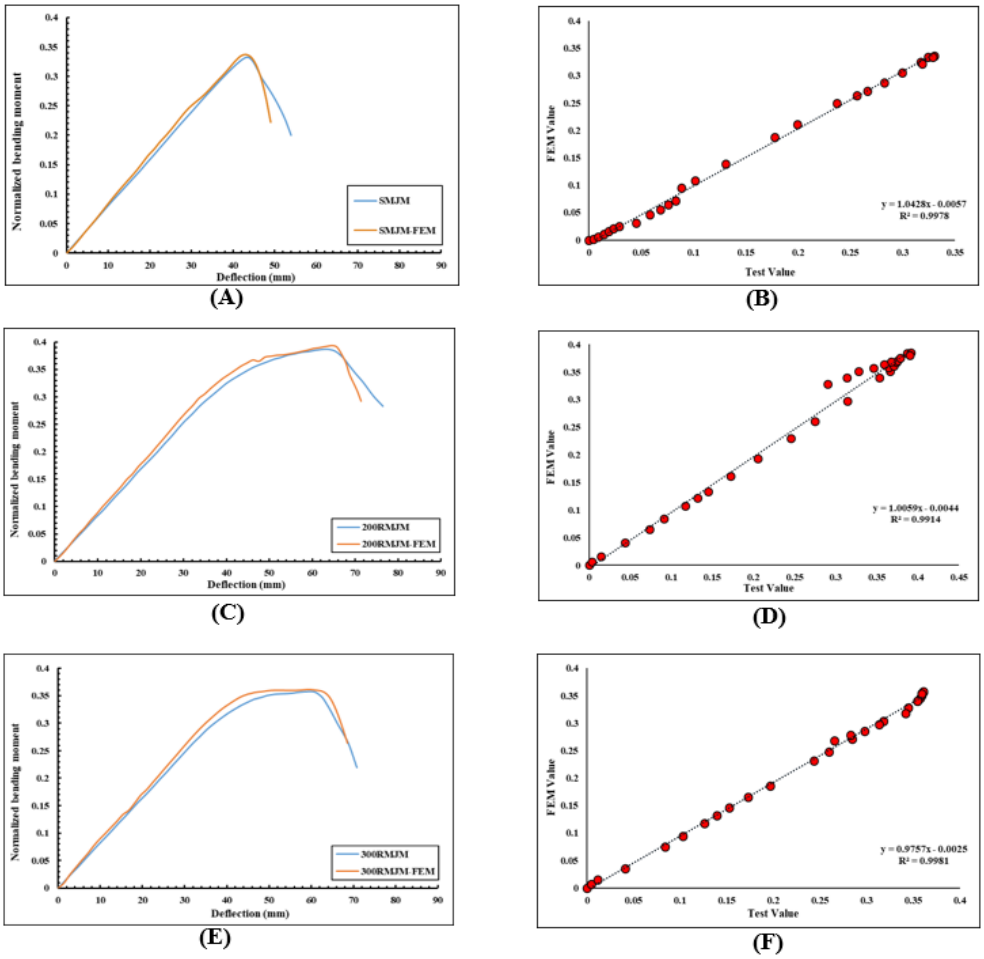

Figure 29. Comparison of finite element model against major axis test results along with the linear regression: (**A**) and (**B**) non-reinforced model; (**C**) and (**D**) 200 mm reinforced model; (**E**) and (**F**) 300 mm reinforced model.

Table 6. Finite element model vs experimental results accuracy details in terms of evaluation criteria.

Non-reinforced model	Evaluation criteria	
	Standard deviation	0.124180809
	Pearson (r)	0.998891538
	R^2	0.9978
200 mm reinforced model	Evaluation criteria	
	Standard deviation	0.135695798
	Pearson (r)	0.995707933
	R^2	0.9914
300 mm reinforced model	Evaluation criteria	
	Standard deviation	0.122399695
	Pearson (r)	0.999038872
	R^2	0.9981

According to Figure 29 and Table 6, the FE results had high accuracy and compatibility with the test results. Figure 30 compares the FE failure modes of the frame with the experimental failure modes where the developed FE model has well predicted the overall deformed shape. These upright frames failed by distortional and local buckling mode.

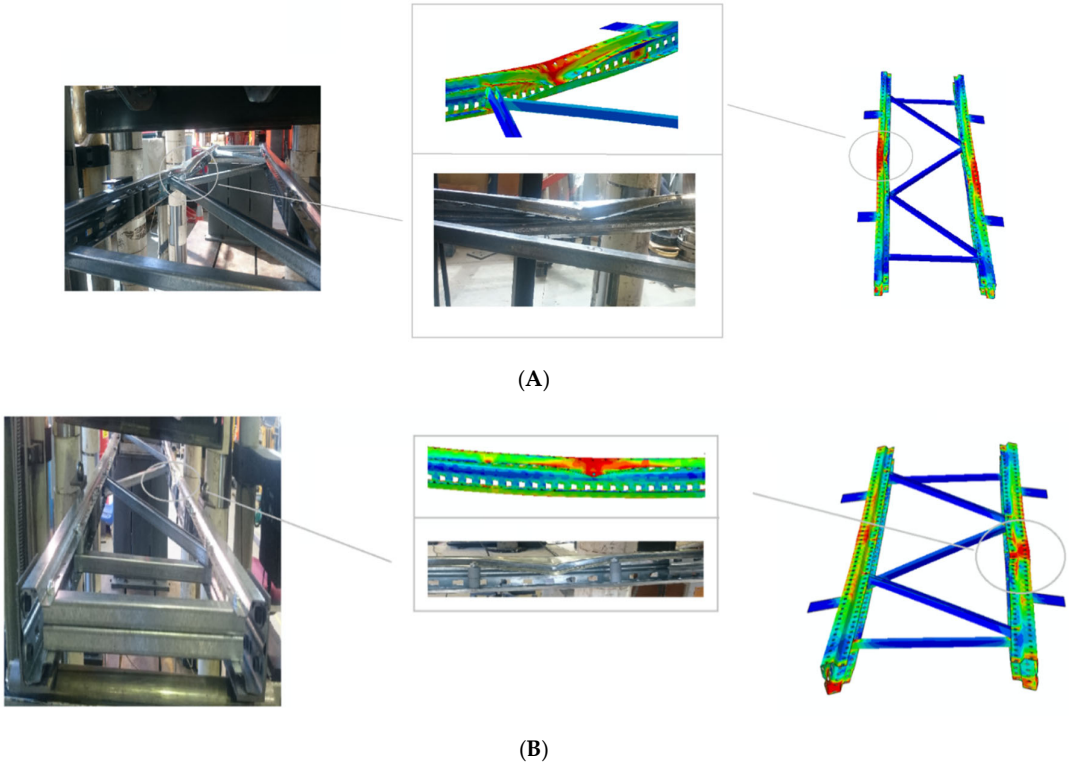

(**A**)

(**B**)

Figure 30. Comparison of failure mode: (**A**) non-reinforced upright type; (**B**) 300 mm reinforced upright type.

6. Conclusions

This study proposed a specific reinforcement system to enhance the flexural strength of CFS upright/beam sections. Eighteen specimens were fabricated and standard monotonic four-point bending displacement control experimental tests were performed to evaluate their bending capacity. All the specimens were made of perforated CFS uprights with 2400 mm length and 1.6 mm thickness. Specimens without reinforcement and specimens with reinforcement at 200 mm and 300 mm pitches were tested about their minor and major axes, respectively. The specimens for the minor axis test consisted of single uprights, while the tested specimens for the major axis tests were produced by combining two uprights as a frame employing conventional diagonal bracing to keep the set-up stable for accurate estimation of the flexural strength of reinforced and unreinforced uprights.

Based on the reported observations, the governing failure modes were local, distortional and a combination of these modes of buckling both in the minor axis and major axis tests. Using the proposed reinforcements increases the bending moment capacity of the specimens by changing the half wavelength of the sections. Reinforcement at 200 mm pitches improves the ultimate flexural capacity compared to the unreinforced specimens by around 13.8% and 17% in major axis and minor axis tests, respectively. Using reinforcement at 300 mm pitches increases the bending moment capacity compared to the unreinforced specimens by 6.97% and 5.5% for the major axis and minor axis tests, respectively. The study emphasized that the proposed reinforcements can be a very useful and cost-effective method for strengthening all open CFS sections under flexural loading, considering the trade-off between flexural performance and the cost of using the method.

Author Contributions: Conceptualization, E.T., A.F. and B.S.; data curation, E.T.; formal analysis, E.T.; funding acquisition, E.T., A.F. and B.S.; investigation, E.T.; methodology, E.T. and B.S.; project administration, E.T. and B.S.; resources, E.T.; software, E.T.; supervision, E.T., A.F., P.M., B.V.H. and B.S.; validation, E.T.; visualization, E.T.; writing—original draft, E.T.; writing—review & editing, E.T.

Funding: The research was funded from R&D contract budget of Western Sydney University. The materials for laboratory testing was provided by Dexion Australia.

Acknowledgments: The authors would like to acknowledge the contribution by Dexion Australia and Professor Hamid Ronagh in supporting this study.

Conflicts of Interest: The authors declare no conflict of interest.

References

1. Taheri, E.; Firouzianhaji, A.; Usefi, N.; Mehrabi, P.; Ronagh, H.; Samali, B. Investigation of a Method for Strengthening Perforated Cold-Formed Steel Profiles under Compression Loads. *Appl. Sci.* **2019**, *9*, 5085, doi:10.3390/app9235085.
2. Chen, C.; Shi, L.; Shariati, M.; Toghroli, A.; Mohamad, E.T.; Bui, D.T.; Khorami, M. Behavior of steel storage pallet racking connection—A review. *Steel Compos. Struct.* **2019**, *30*, 457–469, doi:10.31224/osf.io/jzdpq.
3. Yu, C.; Schafer, B.C. Distortional Buckling Tests on Cold-Formed Steel Beams. *J. Struct. Eng.* **2006**, *132*, 515–528, doi:10.1061/(asce)0733-9445(2006)132:4(515).
4. Calderoni, B.; De Martino, A.; Formisano, A.; Fiorino, L. Cold formed steel beams under monotonic and cyclic loading: Experimental investigation. *J. Constr. Steel Res.* **2009**, *65*, 219–227, doi:10.1016/j.jcsr.2008.07.014.
5. Rogers, C.; Schuster, R. Flange/web distortional buckling of cold-formed steel sections in bending. *Thin Walled Struct.* **1997**, *27*, 13–29, doi:10.1016/0263-8231(96)00017-1.
6. Hancock, G. Design for distortional buckling of flexural members. *Thin Walled Struct.* **1997**, *27*, 3–12, doi:10.1016/0263-8231(96)00020-1.
7. Wang, H.; Zhang, Y. Experimental and numerical investigation on cold-formed steel C-section flexural members. *J. Constr. Steel Res.* **2009**, *65*, 1225–1235, doi:10.1016/j.jcsr.2008.08.007.
8. Wang, L.; Young, B. Beam tests of cold-formed steel built-up sections with web perforations. *J. Constr. Steel Res.* **2015**, *115*, 18–33, doi:10.1016/j.jcsr.2015.08.001.
9. Yuan, W.-B.; Yu, N.-T.; Li, L.-Y. Distortional buckling of perforated cold-formed steel channel-section beams with circular holes in web. *Int. J. Mech. Sci.* **2017**, *126*, 255–260, doi:10.1016/j.ijmecsci.2017.04.001.
10. Moen, C.D.; Schafer, B. Elastic buckling of cold-formed steel columns and beams with holes. *Eng. Struct.* **2009**, *31*, 2812–2824, doi:10.1016/j.engstruct.2009.07.007.
11. Zhao, J.; Sun, K.; Yu, C.; Wang, J. Tests and direct strength design on cold-formed steel channel beams with web holes. *Eng. Struct.* **2019**, *184*, 434–446, doi:10.1016/j.engstruct.2019.01.062.
12. Zhao, O.; Rossi, B.; Gardner, L.; Young, B. Behaviour of structural stainless steel cross-sections under combined loading—Part I: Experimental study. *Eng. Struct.* **2015**, *89*, 236–246, doi:10.1016/j.engstruct.2014.11.014.
13. Dai, L.; Zhao, X.; Rasmussen, L.J. Flexural behaviour of steel storage rack beam-to-upright bolted connections. *Thin Walled Struct.* **2018**, *124*, 202–217, doi:10.1016/j.tws.2017.12.010.
14. Yu, N.-T.; Kim, B.; Yuan, W.-B.; Li, L.-Y.; Yu, F. An analytical solution of distortional buckling resistance of cold-formed steel channel-section beams with web openings. *Thin Walled Struct.* **2019**, *135*, 446–452, doi:10.1016/j.tws.2018.11.012.
15. Zhou, F.; Young, B. Tests of cold-formed stainless steel tubular flexural members. *Thin Walled Struct.* **2005**, *43*, 1325–1337, doi:10.1016/j.tws.2005.06.005.
16. Laím, L.; Rodrigues, J.P.; Da Silva, L.S. Experimental and numerical analysis on the structural behaviour of cold-formed steel beams. *Thin Walled Struct.* **2013**, *72*, 1–13, doi:10.1016/j.tws.2013.06.008.
17. Ye, J.; Hajirasouliha, I.; Becque, J.; Pilakoutas, K. Development of more efficient cold-formed steel channel sections in bending. *Thin Walled Struct.* **2016**, *101*, 1–13, doi:10.1016/j.tws.2015.12.021.
18. Chu, X.-T.; Kettle, R.; Li, L.-Y. Lateral-torsion buckling analysis of partial-laterally restrained thin-walled channel-section beams. *J. Constr. Steel Res.* **2004**, *60*, 1159–1175, doi:10.1016/j.jcsr.2003.11.001.

19. Muftah, F.; Sani, M.S.H.M.; Kamal, M.M.M. Flexural Strength Behaviour of Bolted Built-Up Cold-Formed Steel Beam with Outstand and Extended Stiffener. *Int. J. Steel Struct.* **2018**, *19*, 719–732, doi:10.1007/s13296-018-0157-0.
20. Huang, X.; Yang, J.; Liu, Q.-F.; Zhu, J.; Bai, L.; Wang, F.-L.; Wang, J.-H. A simplified flange–lip model for distortional buckling of cold-formed steel channel-sections with stiffened web. *Int. J. Mech. Sci.* **2018**, *136*, 451–459, doi:10.1016/j.ijmecsci.2017.12.034.
21. Wu, M.-J.; Huang, X.-H.; Zhu, J. Distortional buckling of a CFS channel section with and without stiffened flanges. *J. Mech. Sci. Technol.* **2019**, *33*, 2623–2632, doi:10.1007/s12206-019-0510-z.
22. Visy, D.; Szedlák, M.; Geleji, B.B.; Ádány, S. Flexural buckling of thin-walled lipped channel columns with slotted webs: Numerical and analytical studies. *Eng. Struct.* **2019**, *197*, 109399, doi:10.1016/j.engstruct.2019.109399.
23. Shafaei, S.; Ronagh, H.; Usefi, N. Experimental evaluation of CFS braced-truss shear wall under cyclic loading. In Proceedings of the Advances in Engineering Materials, Structures and Systems: Innovations, Mechanics and Applications, Proceedings Of The 7Th International Conference On Structural Engineering, Mechanics And Computation, September 2-4, 2019, Cape Town, South Africa, UK, 2019; pp. 192–196.
24. Ye, J.; Jiang, L.; Wang, X. Seismic Failure Mechanism of Reinforced Cold-Formed Steel Shear Wall System Based on Structural Vulnerability Analysis. *Appl. Sci.* **2017**, *7*, 182, doi:10.3390/app7020182.
25. Ye, J.; Wang, X. Piecewise Function Hysteretic Model for Cold-Formed Steel Shear Walls with Reinforced End Studs. *Appl. Sci.* **2017**, *7*, 94, doi:10.3390/app7010094.
26. Hancock, G.; Rogers, C. Design of cold-formed steel structures of high strength steel. *J. Constr. Steel Res.* **1998**, *46*, 167–168, doi:10.1016/s0143-974x(98)80013-8.
27. AS 4084. *Steel Storage Racking*; Standards Australia: Sydney, Australia, 2012.
28. Put, B.M.; Trahair, N.S.; Pi, Y.-L. Bending and Torsion of Cold-Formed Channel Beams. *J. Struct. Eng.* **1999**, *125*, 540–546, doi:10.1061/(ASCE)0733-9445(1999)125:5(540).
29. Shariati, M.; Mafipour, M.S.; Mehrabi, P.; Zandi, Y.; Dehghani, D.; Bahadori, A.; Shariati, A.; Trung, N.T.; Shek, P. Application of Extreme Learning Machine (ELM) and Genetic Programming (GP) to design steel-concrete composite floor systems at elevated temperatures. *Steel Compos. Struct.* **2019**, *33*, 319.
30. Shariati, M.; Trung, N.T.; Wakil, K.; Mehrabi, P.; Safa, M.; Khorami, M. Estimation of moment and rotation of steel rack connection using extreme learning machine. *Steel Compos. Struct.* **2019**, *31*, 427–435.
31. Xu, C.; Zhang, X.; Mehrabi, P.; Shariati, A.; Mohamad, E.T.; Hoang, N.; Wakil, K. Using genetic algorithms method for the paramount design of reinforced concrete structures. *Struct. Eng. Mech.* **2019**, *71*, 503–513.
32. Trung, N.T.; Shahgoli, A.F.; Zandi, Y.; Shariati, M.; Wakil, K.; Safa, M.; Khorami, M. Moment-rotation prediction of precast beam-to-column connections using extreme learning machine. *Struct. Eng. Mech.* **2019**, *70*, 639–647.
33. Sedghi, Y.; Sedghi, Y.; Zandi, Y.; Shariati, M.; Ahmadi, E.; Azar, V.M.; Toghroli, A.; Safa, M.; Mohamad, E.T.; Khorami, M.; Wakil, K. Application of ANFIS technique on performance of C and L shaped angle shear connectors. *Smart Struct. Syst.* **2018**, *22*, 335–340.
34. Safa, M.; Shariati, M.; Ibrahim, Z.; Toghroli, A.; Bin Baharom, S.; Nor, N.M.; Petkovic, D. Potential of adaptive neuro fuzzy inference system for evaluating the factors affecting steel-concrete composite beam's shear strength. *Steel Compos. Struct.* **2016**, *21*, 679–688, doi:10.12989/scs.2016.21.3.679.
35. Shariati, M.; Faegh, S.S.; Mehrabi, P.; Bahavarnia, S.; Zandi, Y.; Masoom, D.R.; Toghroli, A.; Trung, N.T.; Salih, M.N.A. Numerical study on the structural performance of corrugated low yield point steel plate shear walls with circular openings. *Steel Compos. Struct.* **2019**, *33*, 569–581.
36. Usefi, N.; Sharafi, P.; Ronagh, H. Numerical models for lateral behaviour analysis of cold-formed steel framed walls: State of the art, evaluation and challenges. *Thin Walled Struct.* **2019**, *138*, 252–285, doi:10.1016/j.tws.2019.02.019.
37. Sharafi, P.; Mortazavi, M.; Usefi, N.; Kildashti, K.; Ronagh, H.; Samali, B. Lateral force resisting systems in lightweight steel frames: Recent research advances. *Thin Walled Struct.* **2018**, *130*, 231–253, doi:10.1016/j.tws.2018.04.019.
38. Sharafi, P.; Rashidi, M.; Samali, B.; Ronagh, H.; Mortazavi, M. Identification of Factors and Decision Analysis of the Level of Modularization in Building Construction. *J. Archit. Eng.* **2018**, *24*, 04018010, doi:10.1061/(asce)ae.1943-5568.0000313.

39. Usefi, N.; Ronagh, H.; Mohammadi, M. Finite Element Analysis of Hybrid Cold-Formed Steel Shear Wall Panels. In *International Structural Engineering and Construction*, 2018; ISEC Press: Fargo, ND, USA, 2018; Volume 5.
40. Cardoso, F.S.; Rasmussen, L.J. Finite element (FE) modelling of storage rack frames. *J. Constr. Steel Res.* **2016**, *126*, 1–14, doi:10.1016/j.jcsr.2016.06.015.
41. Lakusic, S.; Usefi, N.; Nav, F.M.; Abbasnia, R. Finite element analysis of RC elements in progressive collapse scenario. *J. Croat. Assoc. Civ. Eng.* **2016**, *68*, 1009–1022, doi:10.14256/JCE.1550.2016.
42. Majidi, L.; Usefi, N.; Abbasnia, R. Numerical study of RC beams under various loading rates with LS-DYNA. *J. Central South Univ.* **2018**, *25*, 1226–1239, doi:10.1007/s11771-018-3820-x.
43. Usefi, N.; Ronagh, H.; Kildashti, K.; Samali, B. Macro/Micro Analysis of Cold-Formed Steel Members Using ABAQUS and OPENSEES. In *Volume of Abstracts, Proceedings of the 13th International Conference on Steel, Space and Composite Structures (SS18)*; The University of Western Australia: Perth, Australia, 2018.
44. Nav, F.M.; Usefi, N.; Abbasnia, R. Analytical investigation of reinforced concrete frames under middle column removal scenario. *Adv. Struct. Eng.* **2017**, *21*, 1388–1401, doi:10.1177/1369433217746343.
45. Abaqus, V. *6.14 Documentation*; Dassault Systemes Simulia Corporation: Johnston, RI, USA, 2014; Volume 651.